HATLAS-DR2

S.J. Maddox[1] *, et al

ABSTRACT

We present the second public release of source catalogues from the Herschel-ATLAS survey. The catalogued area in this release covers a total of 480 square degrees: 177 square degrees in the north galactic cap, and 303 square degrees in the southern galactic cap. The catalogues contain 114368 and 183784 sources detected at more than 4 sigma significance in any of the 250 μm , 350 μm or 500 μm bands band. The rms positional accuracy for the faintest sources is about 2.4 arc seconds in ra and dec. Photometry is presented for 5 Herschel bands: 100, 160, 250, 350 and 500 μm . We show the distribution of sources as a function of signal-to-noise, and as a function of flux.

Key words:

1 INTRODUCTION

The Herschel mission has revolutionized the study of the FIR sky. The Herschel-ATLAS was the largest project awarded time in the open allocations, and mapped 659 square degrees of sky. The footprint of the survey is spread between 5 disjoint areas: 3 equatorial fields each covering 50 square degrees, giving a total of 161 square degrees; a roughly square region covering 180 square degrees centred on the North Galactic Pole, see Fig 1; and an elongated region covering 318 square degrees in the south galactic cap see Fig 2. The maps and source catalogues for the equatorial fields were described by Valiente et al 2016 (hereafter V16). The creation of maps for the NGP and SGP areas is detailed in the companion paper (Smith et al 2017; hereafter S17). In this paper we describe source detection and catalogues for the NGP and SGP areas. We detect sources and measure their fluxes in areas which are covered by multiple scans by the Herschel detectors, and so the catalogued areas cover 177 square degrees in the NGP, and 303 square degrees in the SGP, slightly smaller than the full area covered by the maps. For the NGP area, identifications to optical sources are presented in a second companion paper (Furlanetto et al 2017; hereafter F17).

   In this paper we describe the process followed to create the source catalogues. In section 2 we describe the source detection process, and our flux measurements; in Section 3 we present our estimates of the flux uncertainties; in Section 4 we show the positional uncertainties; Section 5 discusses the completeness and purity of the source catalogue; Section 6 describes the released catalogue files.
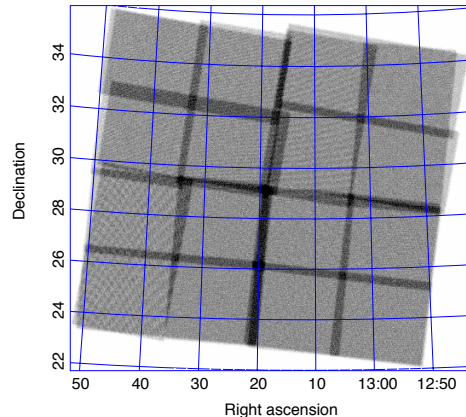
* E-mail: maddoxs@cardiff.ac.uk

Figure 1. The coverage map for 250 μm data in the North Galactic Pole area. The coverage varies from 1 to 43 detector passes with the 5%, median and 95% values being 7, 10 and 16 detector passes. The gray-scale goes from white, 0 passes, to black, 27 passes.

2 SOURCE DETECTION AND CATALOGUES

2.1 Maps and Background subtraction

A detailed description of the processing to produce maps from the Herschel raw data is presented in S17. The resulting maps maps have pixel sizes 3, 4, 6, 8 and 12 arc seconds for 100, 160, 250, 350 and 500 microns respectively. The PACS maps (100 and 160 μm) have units of Jy per pixel. The SPIRE maps have units of Jy per beam and the beam areas are 469, 831 and 1804 square arc seconds.

   Before attempting to detect sources in the maps, we first subtract a smoothly varying 'sky' level to remove the flux contributed by foreground emission from dust in our galaxy, and also by the varying background from clustered sources
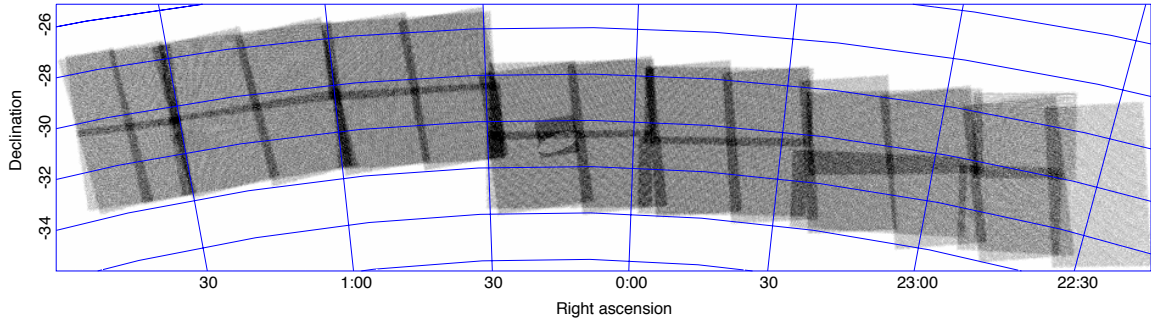
Figure 2. The coverage map for 250 μm data the South Galactic Pole area. The number of detector passes per pixel varies from 1 to 36, with the 5%, median and 95% values being 7, 9 and 14 detector passes with the median of 9 detector passes. In 1, 2, 3 and 4-scan regions the mean number of detector passes is 4.8, 9.6, 14.4 and 19.2. The gray-scale goes from white, 0 passes to black, 21 passes.

fainter than our detection limit. We use the `nebuliser` function from the CASU package to estimate and subtract this background level (see http://casu.ast.cam.ac.uk/surveys-projects/software-release/background-filtering). The filter scales used in `nebuliser` must be small enough to follow relatively small-scale features in some patches of foreground cirrus, but not so small that extended source fluxes are reduced.

For the SPIRE maps we found that a median filter scale of 30 pixels (3 arc minutes in the 250 μm band) followed by a linear filter scale of 15 pixels was an acceptable combination. We tested this by creating simulated maps with large sources and measuring the source fluxes after applying nebuliser. The sources were given exponential profiles truncated at 5 scale-lengths, and then convolved by the SPIRE point spread function. The truncation at 5 scale-lengths corresponds roughly to an optical isophotal radius at μ_r 25mag arcsec^{-2}. The scale-lengths were varied so that the equivalent D25 diameters ranged from 12" to 96". These simulations showed that significant flux is lost only for sources that have diameters larger than 3 arc minutes, and even at this size, the flux loss is $\lesssim 10\%$.

Since the extra-galactic background comes from the sum of clustered distant galaxies, the local background level varies across the sky; the nebuliser background estimate includes this variation, and so will remove it along with foreground emission. Source catalogues made without any background subtraction will include more sources where the background is high from unresolved clusters, and so will have higher apparent clustering than an unbiased flux-limited sample.

For the PACS maps, $1/f$-noise from the instrument is much larger than for SPIRE, so foreground emission is a less significant contribution. This means that we can use a larger nebuliser scale, 5 arc minutes.

The resulting maps have a modal pixel value which is close to zero. For the SPIRE bands, the instrumental noise is low enough that flux distribution of detected sources skews the pixel distribution to positive values so the mean is slightly positive (1.0, 1.0 and 0.6 mJy/beam at 250, 350 and 500 μm). The PACS detector is less sensitive and less stable than SPIRE, and so the instrumental noise dominates over the confusion noise and the pixel distribution is close to Gaussian; the mean of the `nebulised` PACS maps are

very close to zero (0.009mJ/pixel, or 0.016 and 0.016 MJy/str respectively for the 100 and 160 μm maps).

2.2 Source Detection

Sources were detected using the MADX algorithm (Maddox et al in prep) applied to the SPIRE maps. MADX creates maps of the signal-to-noise ratio and identifies sources by finding peaks in the signal to noise. The detection and measurement of fluxes is optimised by using a matched filter that is applied to both the signal map and the noise map.

The SPIRE instrumental noise maps are created from the number of detector passes and the estimated instrumental noise per pass, $\sigma_{inst}/\sqrt{N_{sample}}$, as described in S17 and V16.

Since the noise consists of both instumental noise and confusion noise from the background of undetected sources, we follow the approach of Chapin et al (2011) to calculate the optimal matched filter in each of the three SPIRE bands. Details of estimation and form of the matched filter are discussed in V16. The resulting matched filters are slightly more compact than the corresponding PSFs, and have slightly negative regions outside the FWHM.

In the first step of the source detection, peak pixels which have values $> 2.5\sigma$ in the filtered 250 μm map are considered as potential sources. At this stage only the instrumental noise is included in the noise estimate. The source position is determined by fitting to the pixels around the peak in the 250- μm map. Then the flux in each band is estimated using a bicubic interpolation to the exact position in each filtered map. This means that there is a scatter compared to the original single pixel value, with some sources being assigned fluxes below the original 2.5σ cut. Also, for the 350 μm and 500 μm bands, the scatter can be fairly large, and the estimated fluxes for some low signal-to-noise sources are actually negative. When each source has been measured, a point source profile, scaled to the estimated flux is subtracted from the data, so flux from that source cannot be double-counted in other sources that may be nearby. For each band, sources are sorted in order of decreasing brightness, so that the brighter sources are subtracted from the map before the measurement of fainter sources. Only sources detected above 4 σ in any of the SPIRE bands are retained for the final catalogue. For this cut, the confusion noise as calculated in Section 3
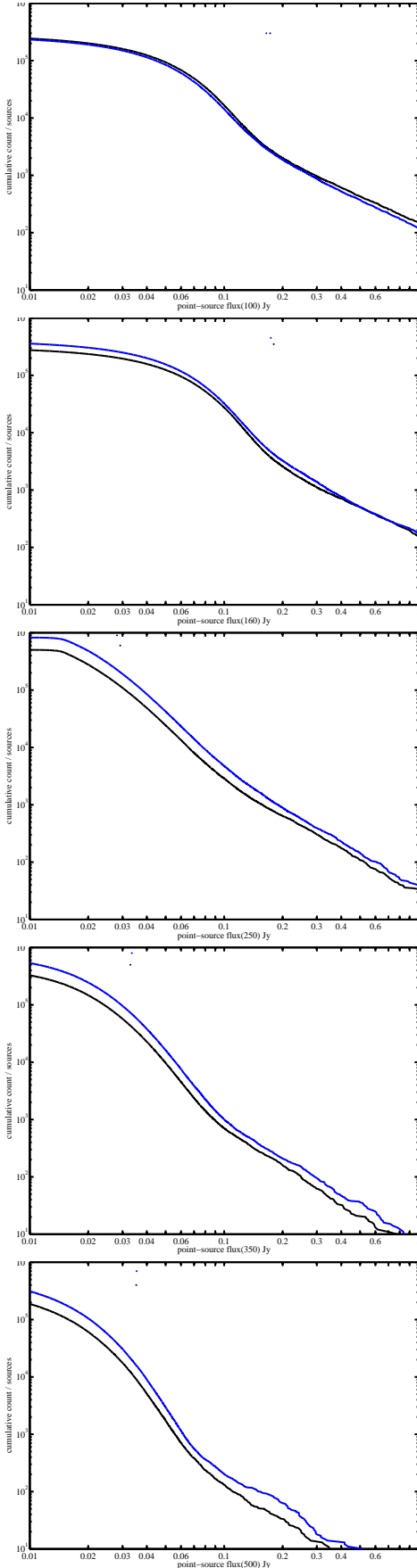
Figure 3. The cumulative number of sources as a function of flux at 100 μm, 160 μm, 250 μm, 350 μm and 500 μm. The NGP field is shown in black; the SGP in blue.

is added in quadrature to the instrumental noise to give an estimate of the total noise.

For the two PACS bands we prefer to use aperture based photometry for all sources, because the PACS psf for our fast-parallel scan mode data is not well determined near the peak. Also the positional uncertainty from the 250 μm detection combined with the higher angular resolution of the PACS maps means that the estimated 250 μm position is likely to miss the peak in PACS map, and hence we would underestimate the flux if we used a matched filter approach as for the longer wavelength SPIRE bands. We set the PACS apertures to have a radius equal to the FWHM of the psf, 11.4 arc seconds for 100 μm and 13.7 arc seconds for 160 μm. These are corrected to total fluxes using the EEF corrections presented in V16, and available at `http://www.h-atlas.org/`. We make a further correction to allow for the bias caused by the expected random positional errors between the SPIRE 250 μm and PACS maps. For sources in the NGP where we have identified a reliable optical counterpart using the maximum likelihood approach presented in F17, we use the optical position to place the apertures, as the optical positions are more precise that the SPIRE 250 μm estimates.

2.3 Extended sources

This approach gives optimal flux estimates for point sources, but will seriously underestimate the flux for extended sources. We use the sizes of optical counterparts to determine which sources are likely to be extended, and sum the flux within an aperture to estimate the total flux of the source. Extended source aperture fluxes are calculated in this way for both PACS and SPIRE bands.

In the NGP area, we use optical identifications with reliability $R > 0.8$, from F17. Sources are considered likely to be extended if the SDSS measured 90% Petrosian radius in the r band, `petroR90_r`, is greater than 8.6 arc seconds. In our previous data release (V16) we based our apertures on the SDSS DR7 `isoA_r`, but this parameter is not available in later SDSS releases. We compared the various radius measures available, and found that a simple scaling of `petroR90_r` provides a robust size measurement that is closely related to `isoA_r`, so `isoA_r` ≈ 1.156 `petroR90_r`. We have simply used the same methods as Valiante et al (2016), but with `isoA_r` replaced by 1.156 `petroR90_r`. So, the radius of the apertures are defined as

$$r_{\mathrm{ap}} = \sqrt{\mathtt{FWHM}^2 + (1.156\,\mathtt{petroR90\_r})^2}\,, \qquad (1)$$

where `FWHM` is the full-width half-max of the point-spread function for the passband being measured.

For the SGP area no SDSS data exists, and we chose to use sizes from the 2MASS survey. We have not performed a full likelihood identification analysis, but have simply looked at the largest galaxies to provide better fluxes for the largest galaxies. In order to derive aperture radii that are similar to the other HATLAS fields, we compared the 2MASS super-coadd 3-sigma isophotal semi-major axis radius to the SDSS `isoA_r` measurements. We found that a simple scaling `isoA_r` ≈ 1.96 `sup_r_3sig` was a reasonable approximation, and so used aperture radii, r_{ap} given by,

$$r_{\mathrm{ap}} = \sqrt{\mathtt{FWHM}^2 + (1.96\,\mathtt{sup\_r\_3sig})^2}\,. \qquad (2)$$

For both the NGP and SGP areas, the aperture flux is used for a source if it is significantly larger than the point-source estimate, ie

$$F_{\mathrm{ap}} - F_{\mathrm{ps}} > \sqrt{\sigma_{\mathrm{ap}}^2 - \sigma_{\mathrm{ps}}^2}\,. \qquad (3)$$

Since the maps have been background subtracted, we do not make any further background subtraction when performing the aperture photometry. We do make a correction to the aperture fluxes to allow for flux outside the aperture using the SPIRE and PACS EEF.

Overall we measure aperture fluxes for 1850 sources in the NGP. For some sources which are barely resolved, the point source flux may be the better flux estimate, and be chose the 'best' flux estimate to be the aperture flux only if it is sginificantly higher than the point source estimate.

We have visually checked the apertures for the largest and brightest sources, and in some cases (how many?) we have adjusted the apertures to better match the Herschel imaging.

2.4   Flux distributions

The observed number of sources as function of flux in the PACS and SPIRES bands is shown in figure 3. The fluxes are subject to boosting as described in V16, and need a statistical de-boosting correction before comparing to model predictions.

2.5   Colour Corrections

The SPIRE maps are calibrated assuming the source spectral energy distribution (SED) varies with frequency as ν^{-1}. For different SED shapes colour corrections K_{ColP} are required, as presented in Tables 5.6 and 5.7 in the SPIRE Handbook.

Since the beam areas depend on the source SED, and extended source photometry depends on maps in Jy/pixel rather than Jy/beam, the extended source fluxes require colour corrections K_{ColP}, as presented in Tables 5.6 and 5.7 in the SPIRE Handbook.

As with SPIRE, the PACS flux density calibrations are based on the assumption that flux density is proportional to ν^{-1}, and a correction is required for sources which follow a different SED. The required corrections are described in the PACS Colour-Correction document[1]).

We have made statistically reliable identifications to optical galaxies from the SDSS and UKIDSS-LAS catalogues, but we have not attempted to produce matched aperture photometry. For the optical photometry from SDSS we use their `ModelMag` measurements; for the NIR photometry from LAS, we use the petrosian magnitude measurements. Both should approximated total magnitudes for the sources, but caution is advised if the photometry is used to constrain the galaxy SEDs without further corrections.

3   FLUX UNCERTAINTIES

3.1   SPIRE point source flux uncertainties

Uncertainties on the flux measurements have been estimated using the methods described in V16. The instrumental noise for each pixel in the maps is estimated from the number of detector passes that contribute to that pixel. The confusion noise was estimated by injecting fake sources to the maps and measuring their fluxes in the same way as for the real data. We found that the confusion noise

---

[1] `http://herschel.esac.esa.int/twiki/pub/Public/PacsCalibrationWeb/cc_report_v1.pdf`

varies as a function of source flux, and we use a simple formula to approximate this:

$$\sigma_{con250}^2 = \min(0.0049, f_{250}/5.6)^2 + 0.00253^2 \qquad (4)$$

For the 350 μm and 500 μm band the confusion noise from the simulated sources is roughly constant, $\sigma_{con350} = 0.00659$ and $\sigma_{con500} = 0.00662$.

The instrumental noise varies over the maps, particularly in areas which are covered by multiple tiles. This can be seen in the histogram of the number of sources as a function of instrumental noise shown in Figure 4. This also shows the histogram of the number of pixels as a function of noise, which is very similar to the histogram of sources, as would be expected for sources roughly uniform over the map. The total noise is the result of adding the instrumental and confusion noise in quadrature.

The peaks in the histogram of noises correspond to areas of different coverage in the maps. The main peak is where there is coverage from the 2-scan regions which have one pair of cross-scan tiles; the second peak is from regions covered by three scans; then next from four scans etc. (see Table 1 from S17).

The variation of noise across the maps means that the total area available varies as a function of the 4 σ flux limit . Figure 5 shows the available area as a function of flux for each of the H-ATLAS fields, including NGP, SGP and equatorial GAMA fields.

The cumulative number of sources as a function of signal-to-noise in the 250 μm detection band is shown in Fig. 6.

3.2   SPIRE extended source flux uncertainties

For extended sources where we have used an aperture flux estimate we have estimated the noise from a Monte-Carlo analysis as described in S17. For 2-scan regions the noise was found to depend on the radius of the aperture as a double power-law,

$$\sigma_{ap}(\mathrm{mJy}) = \begin{cases} Ar^\alpha & \text{if } r \leqslant 50'' \\ B(r-50)^\beta + A50^\alpha & \text{for } r > 50'' \end{cases} \qquad (5)$$

The constants A, B, α, and β are given in Table 3 of S17. For regions covered by more than two scans, the instrumental noise contribution decreases as shown in Table1 of S17, and the change is subtracted in quadrature as shown in Equation 6 of S17.

3.3   PACS flux uncertainties

Our PACS photometry is all based on aperture measurements, so the same approach is used for both point-sources and extended sources. As for SPIRE we estimate the uncertainty of the fluxes by considering random apertures the same size as the point-source apertures. We place three thousand apertures randomly over the 2-scan regions of the maps and calculate summed flux in each; then use the standard deviation of the random aperture sums to provide the one sigma uncertainty estimate. We used radii ranging from the beam FWHM to 100" and found a good fit to the radius dependence is given by a double power law as used for the SPIRE. The values of the constants A, B, α, and β are given in Table 3 of S17. The noise expected for areas covered by more than 2 scans is calculated by assuming that the instrumental noise scales as $1/\sqrt{N_{scan}}$, as shown in Equation 8 of S17.
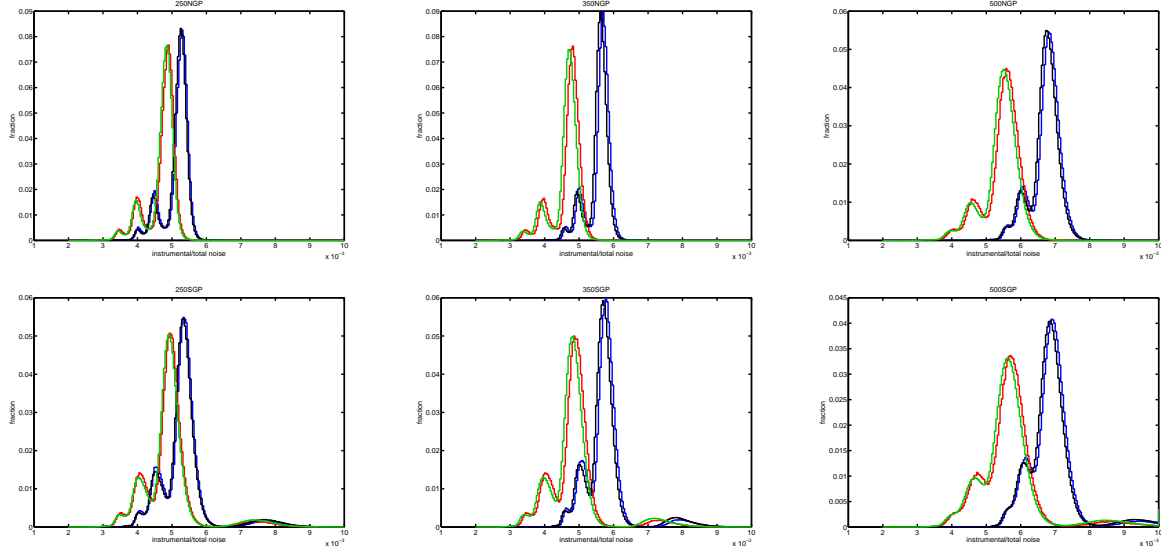
Figure 4. The distribution of instrumental and total noise on the measured 250 μm , 350 μm and 500 μm fluxes for the NGP and SGP fields. Green shows the instrumental noise estimated for each map pixel; red is the instrumental noise for each source; black is the total noise from map pixels, and blue is the total nose for sources. The single scan area is visible as the small peak of sources and pixels with higher noise.

3.4 The distribution of signal to noise ratios

The cumulative distribution of the number of sources as a function of signal to noise for eall five fields and all five bands is shown in Figure 6. The three GAMA fields have similar areas and so have fewer sources in total compared to the NGP and SGP. At the very high signal-to-noise end of the distributions the small number of sources lead to large Poisson errors and large Cosmic variance between the fields, but the overall distribution of noises is very similar between the fields, and so the general shapes of the distributions are very similar.

4 POSITIONAL UNCERTAINTY

Astrometry for the SPIRE maps is calibrated by comparing preliminary source catalogues to SDSS galaxies in the NGP and VST ATLAS in the SGP (see S17). The final source catalogues are thus calibrated to the SDSS and VST astrometric frame. The positional error distribution for the NGP catalogue has been estimated as part of our optical ID process (F17). The distribution of positional offsets is fitted by the expected clustering of galaxies around the FIR galaxies convolved by a Gaussian error distribution. We find that the positional error, $\sigma_{\rm pos}$, varies from 1.2" to 2.4" as the signal-to-noise in flux varies from 10 to 5, so $\sigma_{\rm pos} = 2.4({\rm SNR}/5)^{-0.84}$.

These values of positional uncertainty are consistent with positional errors found in the recovered positions of sources in our simulations (V16).

The mean positional errors as a function of position within the NGP and SGP fields are shown in Fig. 7. Though there are hints of systematic variations in different part of the field, they are typically around the arcsecond level, as expected from the pointing error of the Herschel satellite.

5 COMPLETENESS AND PURITY

To estimate the efficiency of the source detection process we added fake sources to the real maps and re-ran the source detection. We used several thousand sources with fluxes ranging from 6 mJy to 300 mJy, and find that the completeness of our $4-\sigma$ sample is about 90%. More the details of the simulations are described by V16.

The purity of the sample - ie the fraction of apparent sources that correspond to real astronomical sources - is hard to estimate reliably. Since the pixel histogram is highly skewed to positive values, simply inverting the map and counting the number of negative 'sources' does not give a fair measure of the number of noise sources that may be present in the real data. Most of these 'noise' sources will be due to clumps of unresolved faint sources, and not instrumental noise. With the $4-\sigma$ cut, we expect the number of false detections to be $\lesssim 0.5\%$.

REFERENCES

Bertin, E., & Arnouts, S. 1996, AAPS, 117, 393
Clements, D. L., et al. 2010, A&A, in press, arXiv:1005.2409
Driver, S.P., et al., 2009, Astron. Geophys., 50, 5.12
Dunne, L., Eales, S. A., Edmunds, M., Ivison, R., Alexander, P., & Clements, D. L. 2000, MNRAS, 315, 115
Dye, S., et al., 2009 ApJ., 703, 285
Eales, S., et al. 2010, PASP, 122, 499
Griffin et al. 2010 A&A this issue.
Ibar, E., 2010, MNRAS, submitted
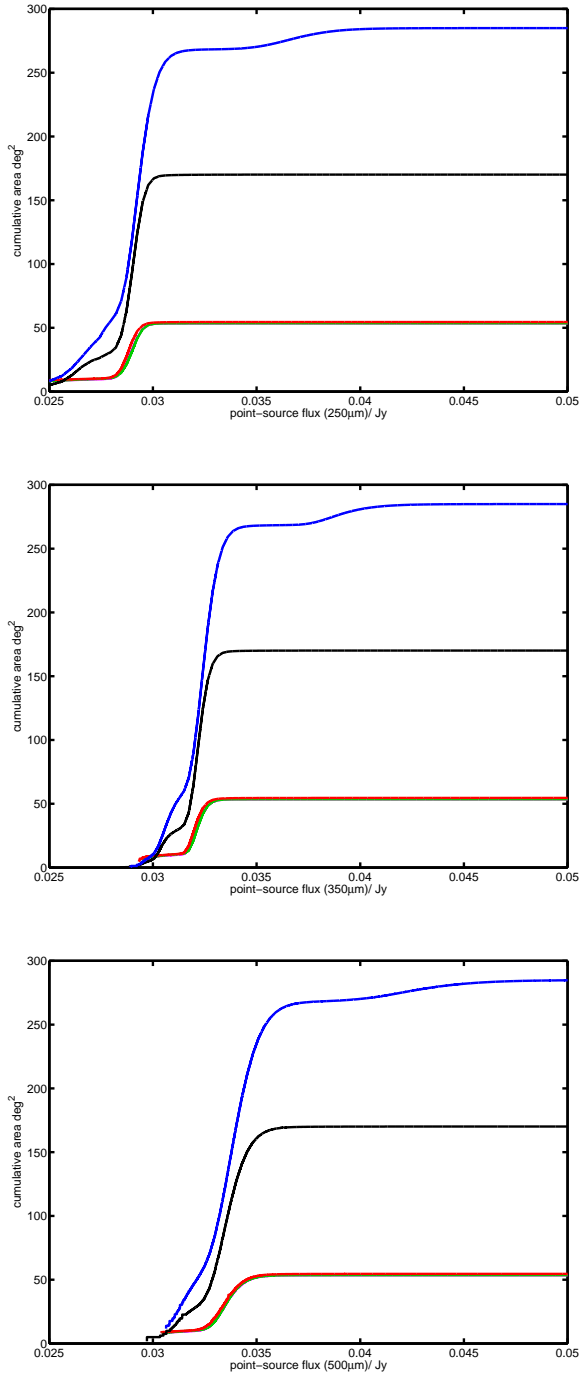Ivison, R. J., et al. 2007, MNRAS, 380, 199

Figure 5. The available survey area as a function of flux limit for the H-ATLAS fields: NGP black; SGP blue; GAMA9 magenta; GAMA12 green; and GAMA15 cyan. The tile overlaps in each field provide deeper areas. In the SGP, the most westerly tile was observed with only one observation for SPIRE, and has no cross-scan data. This means that ∼6% of the area has a higher flux limit, ∼40mJy instead of the typical 28mJy for most of the survey.
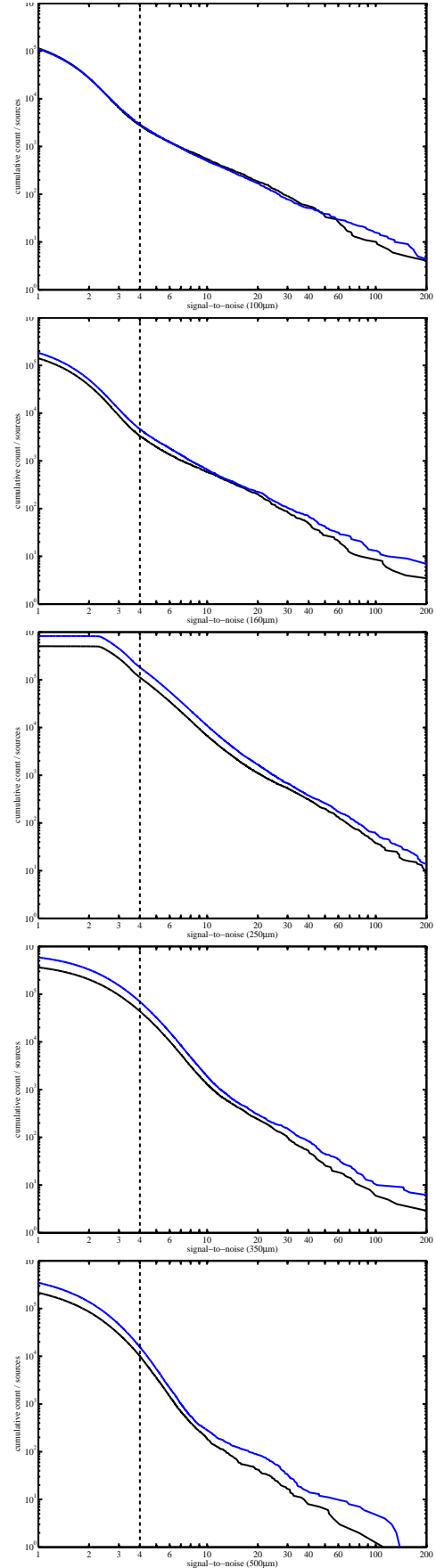

Figure 6. The cumulative number of sources as a function of signal-to-noise at 100 μm , 160 μm , 2250 μm , 350 μm and 500 μm
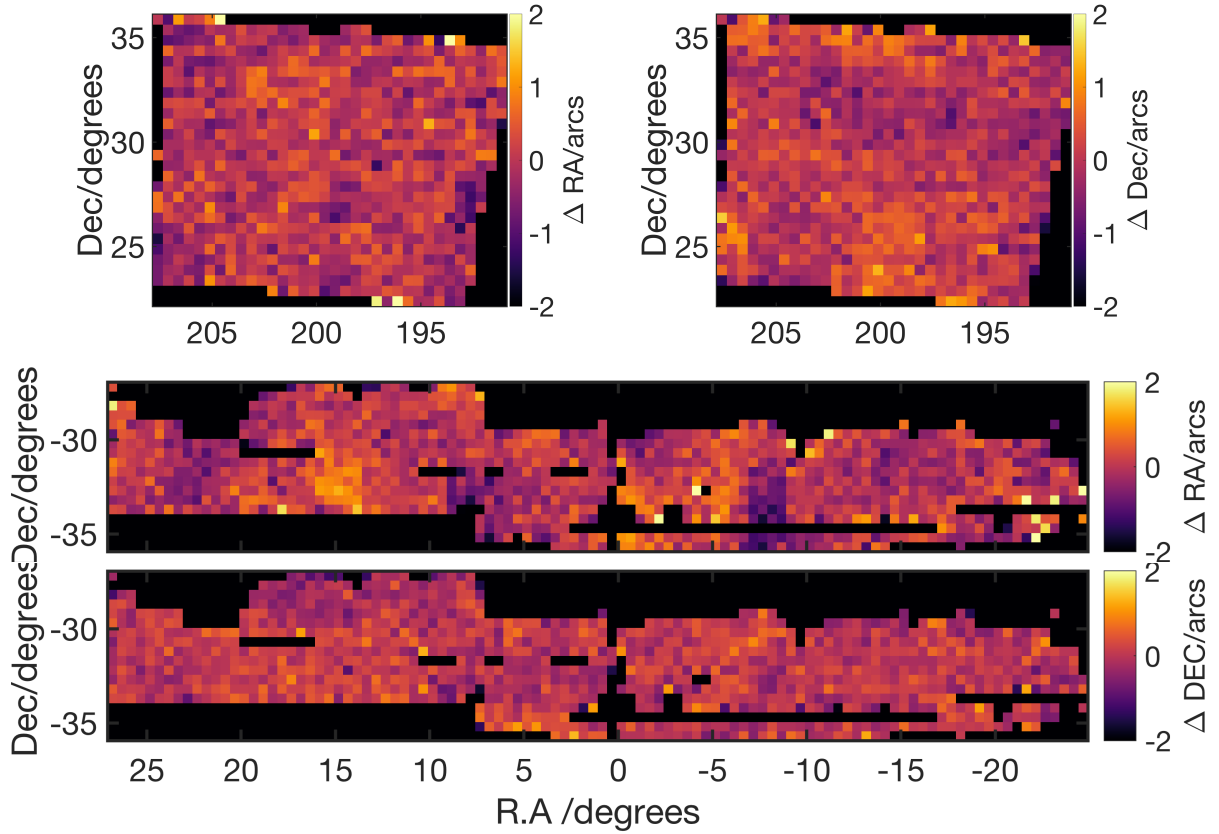
Figure 7. The mean positional errors in R.A and Dec. averaged in 0.5 degree areas as a function of position on the sky for the NGP field and the SGP fields.

Maddox, S. J., et al. 2010, A&A, in press, arXiv:1005.2406

Negrello, M., Perrotta, F., González-Nuevo, J., Silva, L., de Zotti, G., Granato, G. L., Baccigalupi, C., & Danese, L. 2007, MN-RAS, 377, 1557

Ott, S. 2010, in ASP Conference Series, Astronomical Data Analysis Software and Systems XIX, Y. Mizumoto, K.-I. Morita, and M. Ohishi, eds., in press

Pascale, E., et al, 2010, MNRAS, submitted

Pilbratt, G. L., et al. A&A in press, arXiv:1005.5331

Poglitsch, A., et al. 2010 A&A, in press, arXiv:1005.1487

Rigby, E.E, et al., MNRAS.

Rowan-Robinson, M. 2001, in IAU Symp. 204, The Extragalactic Infrared Background and its Cosmological Implications, ed. M. Harwit & M. G. Hauser (Dordrecht: Kluwer), 265

Schlegel, D. J., Finkbeiner, D. P., & Davis, M. 1998, ApJ, 500, 525

Smith, D et al, 2010, MNRAS, in prep

Wang, L., & Rowan-Robinson, M. 2009, MNRAS, 398, 109